Received: 20 July 2021 | Revised: 2 August 2021 | Accepted: 3 August 2021

DOI: 10.1002/mdp2.265

WILEY

REPORT

Dynamic analysis of a Drum Charger: Large amplitude vibrations of clamped circular thin plate on a linear foundation

Fabio Alberti[1] | **Giacomo Risitano**[1] | **Lorenzo Scappaticci**[2] | **Lucas Benoit-Maréchal**[3] | **Danilo D'Andrea**[1]

[1]Department of Engineering, University of Messina, Messina, Italy

[2]Allimep srl, Ponte Felcino (PG), Italy

[3]LMS, École Polytechnique, CNRS, Institut polytechnique de Paris, Palaiseau, France

Correspondence
Danilo D'Andrea, Department of Engineering, University of Messina, Contrada di Dio (S. Agata), 98166 Messina, Italy.
Email: danilo.dandrea@unime.it

Abstract

The Impulse Drum Charger® (IDC) represents a valid and innovative alternative in the field of the superchargers, in particular when the available space is limited, such as in motorcycles. In fact, with respect to the traditional one, which uses turbine-compressor system for engine supercharging, the IDC exploit the deflection of an elastic membrane-spring system to generate overpressure at the intake from the pressure waves generated by the exhaust gases. In this way, the aim of this work is the development of a mathematical model of the membrane-spring system, both realized in 102-RGUD600 glass fiber composite (PA matrix), of a Drum Charger® using Von Karman theory with Berger's approximation. Focusing on the central deflection of the membrane in time and frequency domain, the derived models reproduces with good accuracy the results of the complete finite-element simulations computed with Ansys™, especially in the higher frequencies. Moreover, in order the system work properly, the spring behavior must maintain in linear-elastic range. Hence, a three-point bending test of the spring was carried out, following the specifications in ASTM (D790-03), in order to verify the force-displacement linear relation. The numerical simulations shown excellent agreement with the force-displacement curve observed in the experimental tests.

KEYWORDS

composite material, Drum Charger®, modal analysis, Von Karman theory

1 | INTRODUCTION

Invented at the beginning of the 20th century, turbochargers were initially installed on aircraft engines, which would otherwise stall at high altitudes due to air rarefaction. It is not until the 1970s that the technology was adapted to car engines, revolutionizing Formula One competition and supercar segment. The use of the turbocharger for

supercharging is a very common technique in endothermic engines[1,2] as it allows, by increasing the density of the intake air, to introduce a greater quantity of fresh charge into the cylinder compared to naturally aspirated engines.[3–5] For a given displacement, turbocharging generates more power, with substantial advantages in terms of costs and weight per unit of power delivered. Correspondingly, it is possible to reduce the displacement, thereby decreasing consumption and pollutant emissions, without loss of performance.[6,7]

Nevertheless, if putting a turbo in a car does not pose particular problems, it is a different matter for motorcycles: too big, too complex, and/or too expensive; motorcycle designers have long since abandoned the idea of supercharging their models[8,9] and consequently cannot benefit from the technology to reduce engine emissions. However, the introduction of stricter regulations on emissions has recently led manufacturers to reconsider the application of supercharging to motorcycle engines.

The "Impulse Drum Charger®", a supercharger that uses the pressure waves generated by the exhaust gases to generate overpressure at the intake, provides a compelling solution to the typical limitations of motorcycle engine supercharging. Indeed, it is economical, compact, and, unlike traditional supercharging systems, has a relatively low impact on the plant layout. In fact, even though a redesign of the exhaust system is necessary, it does not require a dedicated lubrication circuit or electronic management. Tests conducted both on the test bench and in real conditions have shown fuel savings from 10% to 30%, attributable to the increase in thermodynamic efficiency and the increase in torque at low revolutions.[10,11]

To achieve effective pressure output, the membrane must compress a sufficient volume of air, which means that its transverse deflection must be many times greater than its thickness. Since the basic linear theory loses its validity in this magnitude range, the geometric nonlinearity introduced by the coupling between axial and transverse motion must be taken into account in order to obtain an accurate solution. The aim of the work is to develop a simple but accurate mathematical model of the membrane-spring system, both realized in 102-RGUD600 glass fiber composite (PA matrix), which will then be included in a global model of the entire Drum Charger®. At the first, experimental three-point bending tests have been conducted on the spring, following the specifications in ASTM (D790-03), in order to verify the force-displacement linear relation. A numerical model of the spring test has been developed through Ansys™ software, comparing the force-displacement characteristic with the experimental tests. After the validation of the numerical model, the information about the spring stiffness have been used for the development of a mathematical model of the membrane-spring system. In particular, three different models, based on Von Karman theory with Berger's approximation, have been taken into account: annular, circular, and full circular model. Also in this case, numerical simulations were carried out using the Ansys™ software, comparing the deflection mode of the membrane with the theoretical models developed.

2 | MATERIAL AND METHODS

The Drum Charger® consists of a very simple geometry. It is a box with two chambers separated by an elastic glass-fiber circular membrane coupled to a leaf spring. One chamber is linked to the exhaust line, the other to the intake duct and the airbox through a series of reed valves[10] (Figure 1).

In order to verify the force-displacement linear characteristic of the spring, three-point bending tests were carried out using an ITALSIGMA's servo-hydraulic load machine (Figure 2A) at a crosshead rate equal to 25 mm/min with constant temperature and relative humidity (23°C and 50% RH). The size of the test specimen was 70 × 20 mm, and the length of span was 100 mm, as per the specifications in ASTM (D790-03) (Figure 2B).

The setup was as follows: initially, the spring rested flat on the cylindrical supports before being pulled up imposing the displacement of its central region (ranging from 0 to 25 mm). For the finite-element simulations with Ansys™, the membrane was modeled as a circular plate clamped on its outer edge with its central region bonded to the spring. The spring rests on two cylindrical steel supports on which it is assumed to move without friction to make the resolution easier (Figure 3).

In fact, given the very small amplitude of the displacement of the spring on the supports, using frictional theory would not impact the results much but would dramatically increase the complexity and therefore, the computation time. Given the thin nature of the membrane and the spring, SHELL181 element has been used for the modeling in Ansys™ simulation. It is a four-noded element with six degrees of freedom at each node (three translations along and three rotations about the x, y, and z directions), suitable for analyzing thin to moderately thick shell structures. It is well-suited for linear, large rotation, and/or large strain nonlinear applications. Besides, the steel cylindrical supports of

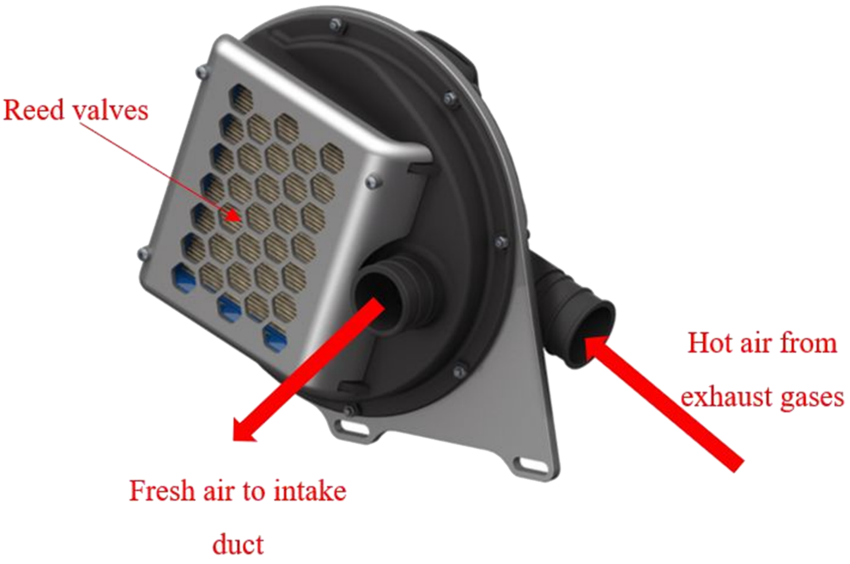

FIGURE 1 Schematic view of IDC

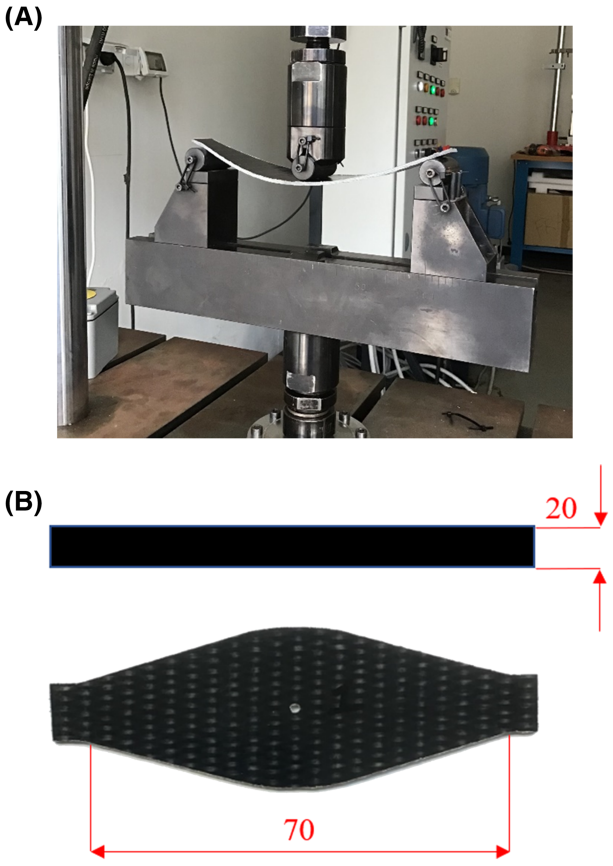

FIGURE 2 Experimental setup: (A) ITALSIGMA's servo-hydraulic load machine during three-point bending test and (B) specimen of the membrane-spring system realized in glass fiber-reinforced epoxy composites

the spring are considered rigid since the Young moduli of the spring and the membrane are one order of magnitude lower than the steel's. Both membrane and spring are realized in 102-RGUD600 glass fiber composite (PA matrix), whose mechanical properties are shown in Table 1.

Considering the behavior of the spring, both from experimental and numerical test, for the development of the membrane-spring system mathematical model, the spring was assumed to be linear. The central deflection of the

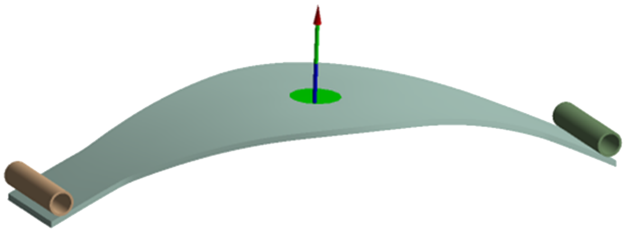

FIGURE 3 Ansys configuration for the spring test

TABLE 1 Mechanical properties of Tepex® dynalite 102-RGUD600(x)/47—PA6-GF67 multidirectional tape

Mechanical properties	Value	Unit
Tensile modulus (parallel and normal)	23,000	MPa
Flexural modulus (parallel and normal)	20,000	MPa
Stress at break (parallel and normal)	390	MPa
Strain at break (parallel and normal)	2.2	%
Flexural strength (parallel and normal)	580	MPa
Density	1800	kg/m^3
Fiber volume content	47	%

membrane in time domain and the maximum amplitude of the deflection in frequency domain have been then compared with the numerical model computed with Ansys™. Due to the moderately large amplitudes, a classical modal analysis is not relevant, as it is based on linear theory. Consequently, all simulations were run using transient analysis to capture the actual deformation of the membrane subjected to a sine wave pressure load. This process is time-consuming (roughly 20 min for a single period) so the analysis was limited to three periods (for an average computation time of 1 h). Therefore, the results need to be considered carefully as it is likely the stationary regime is not reached after three periods. In order for the frequency response curve to be as accurate as possible, simulations have been conducted every 5 Hz ranging from 50 to 150 Hz.

3 | ANALYTICAL MODEL

The equation of motion has been derived relying on a variational approach using Von Karman theory,[12–14] which assumes (i) the quadratic terms of the in-plane strains to be negligible, (ii) the in-plane displacements to be a linear function of the z-coordinate (Love–Kirchhoff hypothesis), and (iii) the out-of-plane displacement to be independent of the z-coordinate. The theory holds for thin plates, that is, $\frac{h}{a} \ll 1$, with h thickness and a radius of the membrane, and moderate rotation ($< 15°$) of the mid-plane normal. In this case, $h/a \sim 4 \times 10^{-}3$ and the maximum rotation is estimated from the Ansys™ solution as $\tan^{-1}(w_0/a) \simeq 5°$.

Let ξ be the displacement field, with ξ_r, ξ_θ, ξ_z its radial, orthoradial, and axial component, respectively[15] (Figure 4).

Further, let u and w be the in-plane and out-of-plane displacements of the middle-plane points. For an axisymmetric deflection, the relations are as follows:

$$\begin{cases} \xi_r(r,z,t) = u(r,t) - z w_{,r}(r,t) \\ \xi_\theta(r,z,t) = 0 \\ \xi_z(r,z,t) = w(r,t) \end{cases} \tag{1}$$

where the comma notation is used for differentiation, that is, $w_{,r} = \frac{\partial w}{\partial r}$.

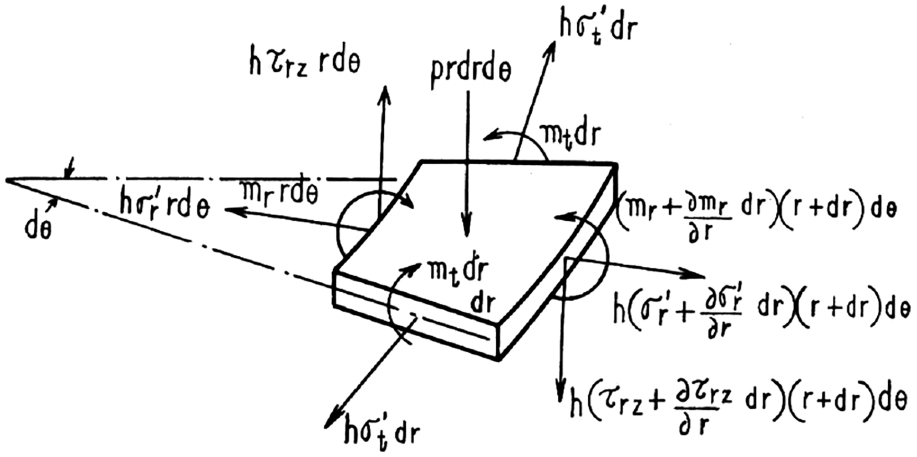

FIGURE 4 Radial, orthoradial, and axial equilibrium condition[15]

Using assumption (i), the Green strain tensor takes the form:

$$\varepsilon = \begin{pmatrix} u_{,r} - z u_{,rr} + \frac{1}{2} w_{,r}^2 & 0 & -w_{,r} \\ 0 & \frac{u - z w_{,r}}{r} & 0 \\ 0 & 0 & \frac{1}{2} w_{,r}^2 \end{pmatrix}. \tag{2}$$

Therefore, for a linear isotropic material in a state of plane stress, where E is the Young modulus, ν Poisson's ratio, $C = Eh/1 - \upsilon^2$ and $D = Eh/12(1 - \upsilon^2)$, the strain energy u, considering the integration domain A (membrane surface), is

$$U = \int_A \frac{1}{2} D \left(w_{,rr}^2 + \frac{w_{,r}^2}{r^2} + 2\nu \frac{w_{,r} w_{,rr}}{r} \right) \mathrm{d}a + \int_A \frac{1}{2} C \left(e_1^2 - 2(1-\nu) e_2 \right) \mathrm{d}a, \tag{3}$$

where has been introduced the first and second invariant of middle surface strains

$$e_1 = u_{,r} + \frac{1}{2} w_{,r}^2 + \frac{u}{r}, \tag{4}$$

$$e_2 = \left(u_{,r} + \frac{1}{2} w_{,r}^2 \right) \frac{u}{r}. \tag{5}$$

Letting σ the surface density of the membrane, the kinetic energy of the membrane is

$$K = \int_A \frac{1}{2} \sigma w_{,t}^2 \, \mathrm{d}a. \tag{6}$$

Likewise, denoting w^s the spring deflection, σ^s its surface density, and A^s its area, the kinetic energy of the spring is

$$K^s = \int_{A^s} \frac{1}{2} \sigma^2 \left(w_{,t}^s \right)^2 \mathrm{d}a. \tag{7}$$

The work of the pressure load p is

$$U^P = \int_A p w \, \mathrm{d}a. \tag{8}$$

The work of the spring force, assuming a point load, is

$$U^k = \frac{1}{2}k(l_0 + w(0,t))^2, \tag{9}$$

where l_0 is the vertical distance between the membrane support and the spring support and k is the spring's stiffness. Therefore, the action of the system is

$$S = \int_{t_1}^{t_2} K + K^s - U - U^p - U^k \mathrm{d}t. \tag{10}$$

To simplify the resolution, the variation of e_2 has been neglected when applying the variational principle (Berger's approximation). Although there is no simple physical justification for this approximation, the comparison of the resulting approximate solution with the available exact solutions shows good agreement,[16–18] especially in the case under investigation where the boundary of the membrane is fixed.[19] Further, modeling the spring as a beam, $w^s(x,t) = w(0,t)\sin(\pi x/L)$ has been assumed for the spring profile, which correspond to the first mode of free vibrations of a simply supported beam. Denoting h^s the spring's thickness and $y(x)$ its width at position x, its kinetic energy then takes the form:

$$K^s = \frac{\sigma}{2}\frac{h^s}{h}\left(\int_0^L y(x)\sin^2\left(\frac{\pi x}{L}\right)\mathrm{d}x\right)\left(\int_A w_{,t}^2 \frac{\delta(r)}{2\pi r}\,\mathrm{d}a\right). \tag{11}$$

After renormalization of the different quantities as

$$\overline{r} = \frac{r}{a}, \overline{w} = \frac{w}{h}, \overline{l_0} = \frac{l_0}{h}, \overline{t} = \frac{t}{a^2\sqrt{\sigma/D}}, \overline{p} = \frac{a^4}{Dh}p, \overline{k} = \frac{a^2}{D}k \tag{12}$$

the following equations are obtained, where we have dropped the overlines for conciseness,

$$\begin{cases} e_{,r} = 0 \\ \Delta^2 w - 12e\Delta w + \left(1 + \alpha\dfrac{h^s}{h}\dfrac{\delta(r)}{2\pi r}\right)w = p - k(l_0 + w(0,t))\dfrac{\delta(r)}{2\pi r}, \end{cases} \tag{13}$$

where from the spring shape,

$$\alpha = \frac{1}{a^2}\int_0^L y(x)\sin^2\left(\frac{\pi x}{L}\right)\mathrm{d}x \simeq 0.67.$$

Recalling $(0) = u(1) = 0$, the constant E can be evaluated to

$$\int_0^1 er\,dr = \int_0^1 (ru_{,r} + u)\,dr + \frac{1}{2}\int_0^1 \omega_{,r}^2 r\,dr \Rightarrow e = 2[ra]_0^1 + \int_0^1 w_{,r}^2 r\,dr \tag{14}$$

Finally, adding a damping term $w_{,t}$:

$$\Delta^2 w - 12e\Delta w + \left(1 + \alpha\frac{h^s\,\delta(r)}{h\,2\pi r}\right)w_{,tt} + \mu w_{,t} = p - k(l_0 + w(0,t))\frac{\delta(r)}{2\pi r}. \tag{15}$$

Equation 15 has been solved by the Galerkin method, using the modal functions R_n from the linearized small vibration problem as shape functions, that is, $w(r,t) = \sum_n R_n(r)\tau_n(t)$. By definition, $\Delta^2 R_n = \omega_n^2 R_n$ and therefore, introducing the Bessel function of the first kind J_α and the modified Bessel function of the first kind I_α:

$$R_n(r) = J_0(\lambda_n r) - \frac{J_0(\lambda_n)}{I_0(\lambda_n)} I_0(\lambda_n r) \tag{16}$$

where the $\lambda_n = \sqrt{\omega_n}$ are the solutions to $J_0(r)I_1(r) - J_1(r)I_0(r) = 0$.

After application of the Galerkin method, Equation 15 takes the form, for $i,j \in \{1,2\}$:

$$\sum_j \left[\int_0^1 R_i(r)R_j(r)r\,\mathrm{d}r + \frac{\alpha\, h^s}{2\pi\, h} R_i(0)R_j(0)\right]\ddot{\tau}_j + \mu \sum_j \left[\int_0^1 R_i(r)R_j(r)r\,\mathrm{d}r\right]\tau_j + 12\sum_{j,k,l}\left[\int_0^1 R_k'(r)R_l'(r)r\,\mathrm{d}r \int_0^1 R_j'(r)R_i'(r)r\,\mathrm{d}r\right]\tau_j\tau_k\tau_l$$
$$+ \sum_j \left[\omega_j^2 \int_0^1 R_j(r)R_i(\mathrm{r})r\,\mathrm{d}r + kR_j(0)R_i(0)\right]\tau_j$$
$$= \left[\int_0^1 R_i r\,\mathrm{d}r\right] p - \frac{k}{2\pi} l_0 R_i(0),$$

where $r_0 = \begin{cases} 0 & \text{for the circular model} \\ \dfrac{b}{a} & \text{for the annular model} \end{cases}$.

Hence, it is possible to compare three different models with the Ansys™ numerical simulation: annular, circular and full circular model.

4 | VALIDATION OF THE MODEL

All the results evaluated from experimental, analytical, and numerical simulations have been investigated, focusing in particular on:

- Comparison between experimental and numerical results of the spring behavior.
- Comparison between analytical and numerical model of the membrane deflection in time and frequency domain;

4.1 | Spring behavior comparison (experimental and numerical simulation)

The comparison between experimental and numerical results of the force-displacement characteristic of the spring are in excellent agreement (Figure 5) and show that the spring behaves approximately linearly with an equivalent stiffness of 10,412 N/m.

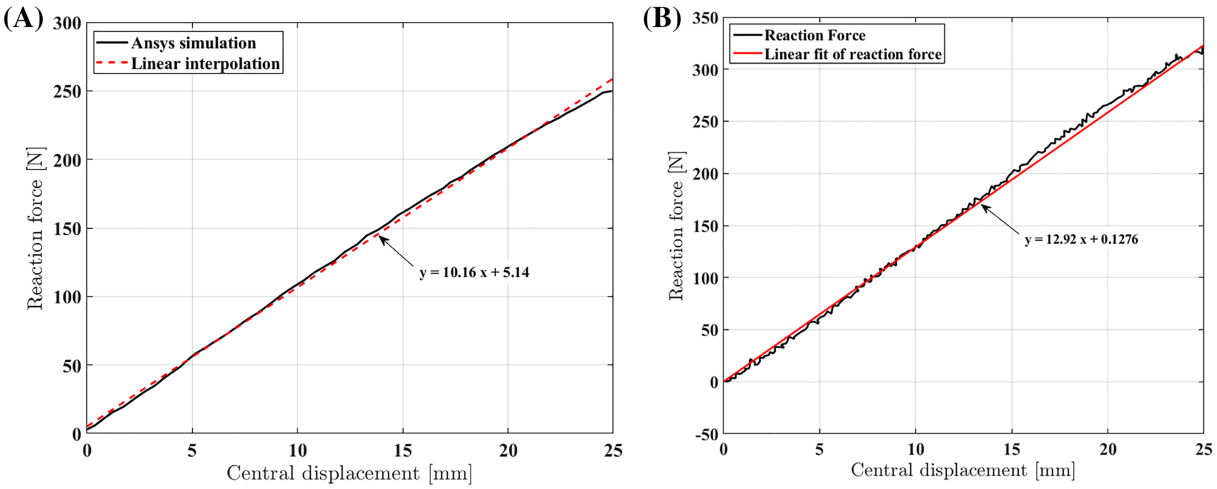

FIGURE 5 Characteristic of the spring: (A) obtained from Ansys simulation and (B) obtained from experimental test

4.2 | Membrane deflection comparison (analytical and numerical simulation)

Based on the first computed values of the modal frequencies (Table 2), it is possible to justify why a two-mode approximation is coherent with the case study.

Indeed, since the Drum Charger® draws its power from the exhaust gases, its working frequency will roughly be the same as the engine's (combustion takes place once every two rotations in one cylinder but with multiple cylinders the combustion cycles are not synced), that is, from 3000 to 9000 rpm, which correspond to a frequency range of 50–150 Hz. As a result, the second mode (≈ 208 Hz), although out of the range, will be partly excited, while the third and higher ones (> 465 Hz) are too high in frequency to have a significant impact on the result. This is also confirmed by the deflection shape of the membrane observed in the numerical simulation, where the second mode, with one circular node, is evident (Figure 6C).

TABLE 2 Modal frequencies for the first four modes

Mode	1	2	3	4
Full circular model frequency (Hz)	53.368	207.765	465.481	826.356
Circular model frequency (Hz)	63.259	246.271	551.751	979.509
Annular model frequency (Hz)	53.102	205.874	466.480	840.449

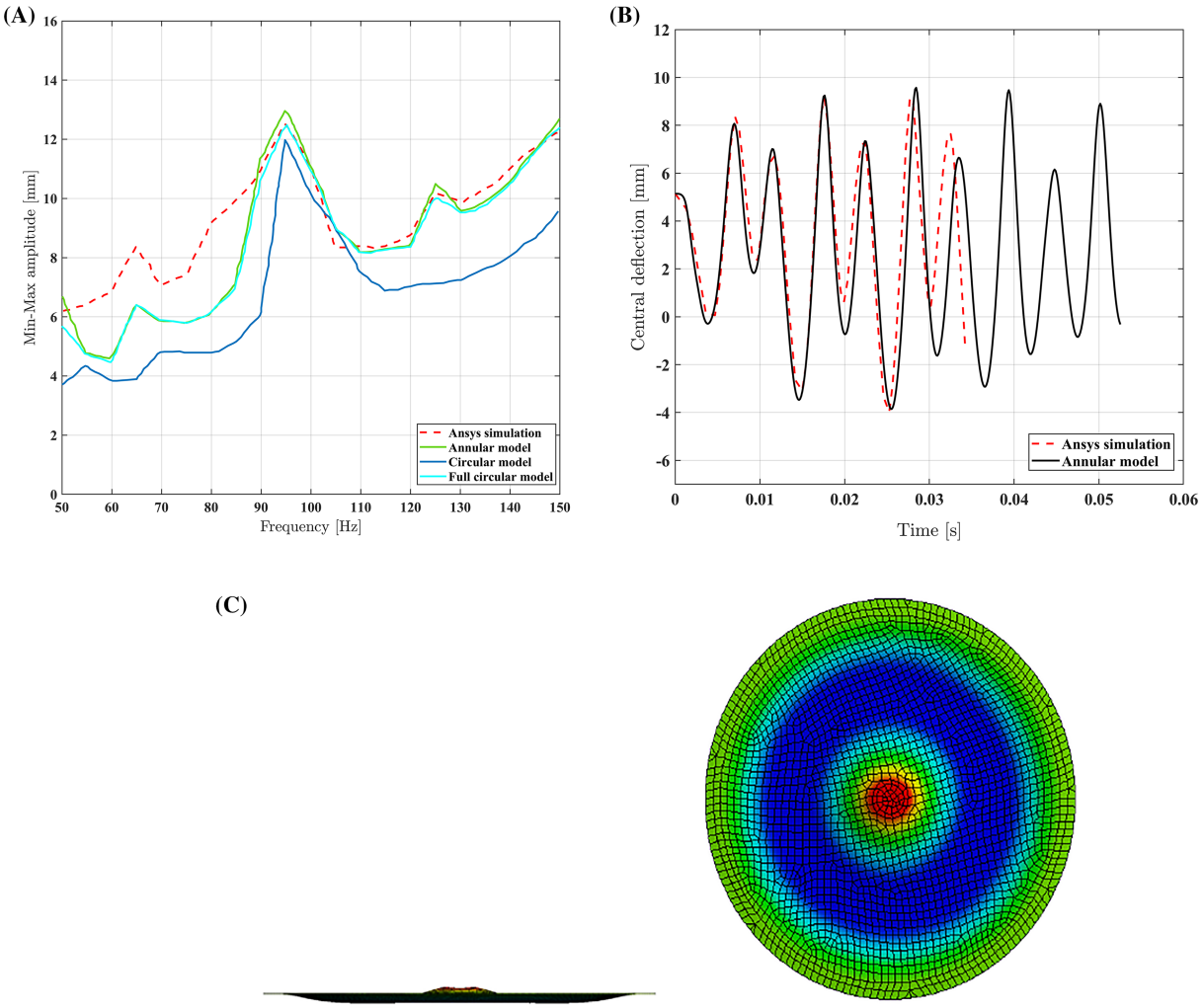

FIGURE 6 Analytical and numerical results of the membrane deflection. (A) Frequency response. (B) Time response at 95 Hz of the annular model. (C) Second mode evidence of the numerical simulation

The numerical simulations of this simplified model are in very good agreement with the complete finite-element simulations in the high-frequency domain, that is, after the resonance peak (Figure 6A). The curves are almost perfectly superimposed, with the right values of displacement at 95, 125, and 150 Hz (Figure 6A), and otherwise underestimated by 11% at most.

As before, the two-mode approximation remains justified (see Table 2). Is possible to notice that the full circular model and the annular model yield almost the same results, whereas the circular plate, as expected given its smaller radius, presents a much stiffer behavior: the displacement observed is much smaller and the resonance peak is shifted towards the higher frequencies compared to the other models (see Figure 6). The great similarity observed between the first two models is only logical: since the bonding region's radius is small compared to the membrane's total radius, the annular plate is actually well approximated by a full circular plate (the closer the radius gets to 0, the closer the annular plate's behavior gets to the full circular plate's).

In the low-frequency domain however, the response is not quite as satisfactory. The whole frequency response is offset 2 mm lower than what it should be. Besides, it is possible to identify an additional secondary resonance peak at 50 Hz, which is completely absent in the Ansys simulations. Given the simplicity of the model, deviations from the finite-element simulations are expected. It is remarkable that it captures so well the high-frequency dynamics, but a more refined model of the spring and/or membrane would be necessary to capture the low-frequency response more accurately.

5 | CONCLUSION

In this work, a theoretical model of the membrane-spring system of a Drum Charger® has been derived and compare it to complete finite-elements simulations computed with Ansys™. The spring behavior was assessed experimentally through a three-point bending test that showed a linear force-displacement response, in excellent agreement with the numerical simulations. Using Von Karman theory with Berger's approximation, the membrane is modeled as a clamped circular plate with its central region bound to the spring. Based on the working regime of the engine, the analysis is restrained to the two lowest vibration modes. Comparison to the numerical simulations show that the theoretical model accurately predicts the membrane response at high frequencies but lacks precision in the lower frequencies.

CONFLICT OF INTEREST

The authors declare no conflict of interest.

DATA AVAILABILITY STATEMENT

The data that support the findings of this study are available from the corresponding author upon reasonable request.

ORCID

Fabio Alberti https://orcid.org/0000-0003-2457-8344
Giacomo Risitano https://orcid.org/0000-0002-0506-8720
Lorenzo Scappaticci https://orcid.org/0000-0001-6393-8037
Danilo D'Andrea https://orcid.org/0000-0002-9809-8434

REFERENCES

1. Zinner KA. *Supercharging of Internal Combustion Engines: Additional Chapter 12*. Berlin, Germany: Springer Science & Business Media; 2012.
2. Lee W, Schubert E, Li Y, Li S, Bobba D, Sarlioglu B. Overview of electric turbocharger and supercharger for downsized internal combustion engines. *IEEE Trans Transp Electrif*. 2016;3(1):36-47.
3. Hiereth H, Prenninger P. *Charging the Internal Combustion Engine*. Berlin, Germany: Springer Science & Business Media; 2007.
4. Attard W, Watson HC, Konidaris S, Khan MA. Comparing the performance and limitations of a downsized formula SAE engine in normally aspirated, supercharged and turbocharged modes. SAE Technical Paper; 2006.
5. Mahmoudi AR, Khazaee I, Ghazikhani M. Simulating the effects of turbocharging on the emission levels of a gasoline engine. *Alex Eng J*. 2017;56(4):737-748.
6. Mishra S, Anand K, Santhosh S, Mehta PS. Comparison of biodiesel fuel behavior in a heavy duty turbocharged and a light duty naturally aspirated engine. *Appl Energy*. 2017;202:459-470.
7. Lecointe B, Monnier G. Downsizing a gasoline engine using turbocharging with direct injection. SAE Technical Paper; 2003.

8. Zinner C, Abart M, Schögl O, Leiber S, Schabetsberger T. Charging and powersport for motorcycles: a contradiction? SAE Technical Paper; 2011.
9. Shakti P. Performance calculation & development of turbocharged gasoline direct injection 125cc motorcycle engine. *Int J Mech Mater Eng*. 2018;2(1):23-32.
10. Cruccolini V, Discepoli G, Zembi J, Battistoni M, Mariani F, Grimaldi CN. Experimental assessment of a pressure wave charger for motorcycle engines. *Energy Procedia*. 2018;148:1254-1261. https://doi.org/10.1016/j.egypro.2018.08.002
11. Starodetko KE, Simand S, Drobychevskj TB, et al. High performance characteristics of a motorcycle powered by a four-stroke small 50cc-125cc engine at the expense of a positive displacement air compressor as a supercharger. SAE Technical Paper 2013; 2013: https://doi.org/10.4271/2013-32-9015
12. GhannadPour SAM, Alinia MM. Large deflection behavior of functionally graded plates under pressure loads. *Compos Struct*. 2006; 75(1-4):67-71. https://doi.org/10.1016/j.compstruct.2006.04.004
13. Yu Q, Xu H, Liao S. Coiflets solutions for Föppl-von Kármán equations governing large deflection of a thin flat plate by a novel wavelet-homotopy approach. *Numer Algorithms*. 2018;79(4):993-1020. https://doi.org/10.1007/s11075-018-0470-x
14. Chen JK, Sun CT. Dynamic large deflection response of composite laminates subjected to impact. *Compos Struct*. 1985;4(1):59-73. https://doi.org/10.1016/0263-8223(85)90020-0
15. Way S. Bending of circular plates with large deflection. *Trans ASME*. 1934;54:627-636.
16. Kaak E, Bikri E. Large vibration amplitude of circular functionally graded plates resting on Pasternak foundations. *Int J Mech Mechatronics Eng*. 2013;7(9):1816-1820. https://doi.org/10.5281/zenodo.1087800
17. Benamar R, Bennouna MMK, White RG. The effects of large vibration amplitudes on the mode shapes and natural frequencies of thin elastic structures, part II: fully clamped rectangular isotropic plates. *J Sound Vib*. 1993;164(2):295-316. https://doi.org/10.1006/jsvi.1993.1215
18. El Kadiri M, Benamar R, White RG. The non-linear free vibration of fully clamped rectangular plates: second non-linear mode for various plate aspect ratios. *J Sound Vib*. 1999;228(2):333-358. https://doi.org/10.1006/jsvi.1999.2410
19. Sarker, P.K. On the large deflection analysis of circular plates of variable thickness with edges elastically restrained against rotation. 1981.

How to cite this article: Alberti F, Risitano G, Scappaticci L, Benoit-Maréchal L, D'Andrea D. Dynamic analysis of a Drum Charger: Large amplitude vibrations of clamped circular thin plate on a linear foundation. *Mat Design Process Comm*. 2021;3(5):e265. doi:10.1002/mdp2.265